Fine-tuning of p-coumaric acid synthesis to increase (2S)-naringenin production in yeast

Metabolic Engineering 79 (2023) 192–202

Contents lists available at ScienceDirect

Metabolic Engineering

journal homepage: www.elsevier.com/locate/meteng

Fine-tuning of *p*-coumaric acid synthesis to increase (2*S*)-naringenin production in yeast

Jiwei Mao [a], Marta Tous Mohedano [a], Jing Fu [a], Xiaowei Li [a], Quanli Liu [a], Jens Nielsen [a,b], Verena Siewers [a], Yun Chen [a,*]

[a] Department of Life Sciences, Chalmers University of Technology, SE412 96 Gothenburg, Sweden
[b] BioInnovation Institute, DK2200, Copenhagen N, Denmark

ARTICLE INFO

Keywords:
Synthetic biology
Metabolic engineering
Dynamic control
Intermediate distribution
Natural products

ABSTRACT

(2*S*)-Naringenin is a key precursor for biosynthesis of various high-value flavonoids and possesses a variety of nutritional and pharmaceutical properties on human health. Systematic optimization approaches have been employed to improve (2*S*)-naringenin production in different microbial hosts. However, very few studies have focused on the spatiotemporal distribution of (2*S*)-naringenin and the related pathway intermediate *p*-coumaric acid, which is an important factor for efficient production. Here, we first optimized the (2*S*)-naringenin biosynthetic pathway by alleviating the bottleneck downstream of *p*-coumaric acid and increasing malonyl-CoA supply, which improved (2*S*)-naringenin production but significant accumulation of *p*-coumaric acid still existed extracellularly. We thus established a dual dynamic control system through combining a malonyl-CoA biosensor regulator and an RNAi strategy, to autonomously control the synthesis of *p*-coumaric acid with the supply of malonyl-CoA. Furthermore, screening potential transporters led to identification of Pdr12 for improved (2*S*)-naringenin production and reduced accumulation of *p*-coumaric acid. Finally, a titer of 2.05 g/L (2*S*)-naringenin with negligible accumulation of *p*-coumaric acid was achieved in a fed batch fermentation. Our work highlights the importance of systematic control of pathway intermediates for efficient microbial production of plant natural products.

1. Introduction

Flavonoids are the largest classes of polyphenolic secondary metabolites in plants, representing an important resource of therapeutics and nutraceuticals due to their antioxidant, anti-inflammatory, anti-tumor activities, liver-protective properties as well as memory enhancement (Birt et al., 2001; Panche et al., 2016). (2*S*)-Naringenin is one of the most important scaffolds for producing a wide variety of subgroups of flavonoids, such as flavones, flavonols, isoflavones, anthocyanins. Numerous investigations also demonstrated the beneficial effects of (2*S*)-naringenin to many human pathological conditions, including obesity, cancer, diabetes, Alzheimer's disease and coronavirus (Clementi et al., 2021; Manchope et al., 2017; Salehi et al., 2019). It is therefore of great interest to engineer microbial cells for efficient production of (2*S*)-naringenin and its derivatives. The formation of (2*S*)-naringenin begins with the conversion of L-tyrosine or L-phenylalanine to *p*-coumaric acid (also called *p*-hydroxycinnamic acid, *p*HCA) through the action of tyrosine ammonia lyase (TAL) or phenylalanine ammonia lyase (PAL) combined with cinnamic acid hydroxylase (C4H). *p*-Coumaric acid is subsequently converted by *p*-coumaroyl-CoA ligase (4CL) to form 4-coumaroyl-CoA. Next, one molecule of 4-coumaroyl-CoA is condensed with three molecules of malonyl-CoA to generate naringenin chalcone by a type III polyketide synthase, chalcone synthase (CHS). In the final step, the naringenin chalcone is converted to (2*S*)-naringenin by the action of chalcone isomerase (CHI) (Fig. 1A).

For microbial-based production of (2*S*)-naringenin, its biosynthetic pathway has been reconstituted into different hosts including *Escherichia coli* (Dunstan et al., 2020; Zhou et al., 2021), *Corynebacterium glutamicum* (Kallscheuer et al., 2016), *Streptomyces venezuelae* (Park et al., 2009), *Yarrowia lipolytica* (Palmer et al., 2020; Wei et al., 2020) and *Saccharomyces cerevisiae* (Gao et al., 2020a; Koopman et al., 2012; Li et al., 2021; Zhang et al., 2021). Progress has been made to improve (2*S*)-naringenin production by supplementation of precursor amino acids (L-tyrosine, L-phenylalanine) or *p*-coumaric acid, or by *de novo*

* Corresponding author.
E-mail address: yunc@chalmers.se (Y. Chen).

https://doi.org/10.1016/j.ymben.2023.08.003
Received 11 May 2023; Received in revised form 3 August 2023; Accepted 20 August 2023
Available online 22 August 2023

synthesis from simple carbon sources like glucose. Most efforts have been centered on balancing the (2*S*)-naringenin biosynthetic pathway, including modular pathway engineering (Lv et al., 2019; Lyu et al., 2017; Wu et al., 2014), promoter and RBS engineering (Gao et al., 2020b; Zhou et al., 2019), or a riboswitch-guided screening approach (Hwang et al., 2021). Also, different genetic circuits have been constructed for dynamic control of malonyl-CoA supply and (2*S*)-naringenin production (Wu et al., 2021; Zhou et al., 2021), or for metabolic flux control based on quorum-sensing (Dinh et al., 2020; Dinh and Prather, 2019). However, very few studies have focused on the accumulation and distribution of its intermediates such as *p*-coumaric acid and the product (2*S*)-naringenin. This can be a critical factor for developing efficient biotechnological processes to produce them. For example, the efficient export of pathway intermediates will result in lower intracellular concentrations, which can be deleterious to the metabolic flux through the pathway especially for downstream slower enzymatic steps (Jamil et al., 2022). At the same time, this exportation can also lead to carbon loss and accumulation of toxic intermediates, which are important obstacles that hinder efficient microbial production (Tous Mohedano et al., 2023; Wang et al., 2021).

In plants, the biosynthesis, storage, and function of secondary metabolites to fulfill their biological roles often involve different cellular localizations and processes. The subcellular translocation of secondary metabolites is likely to occur by active transport processes, but the specific transporters involved have not been satisfactorily identified (Zhao, 2015; Zhao and Dixon, 2010). Furthermore, when transferring

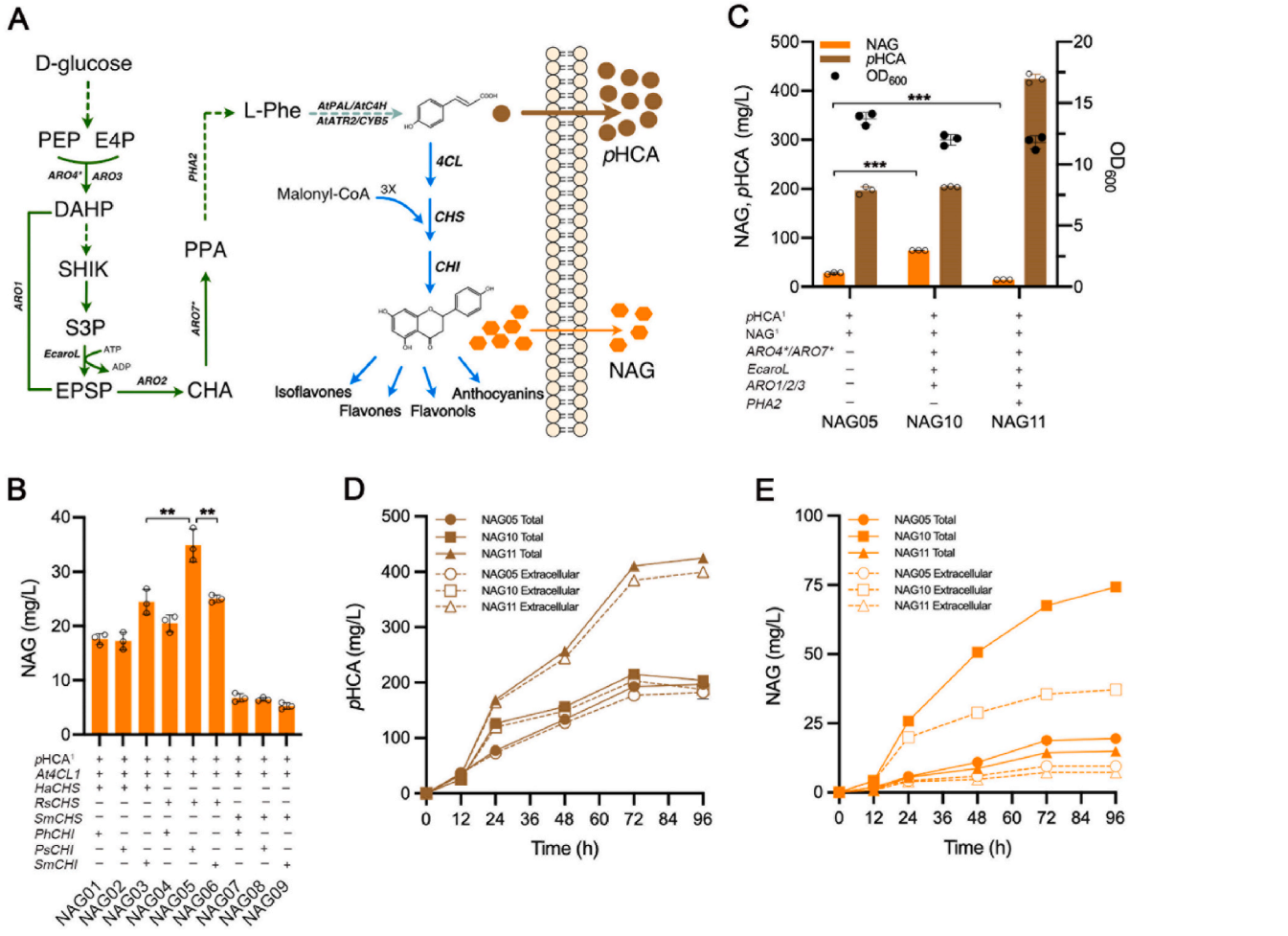

Fig. 1. Extracellular accumulation of *p*-coumaric acid limits (2*S*)-naringenin biosynthesis. (A) Schematic diagram of the biosynthetic pathway leading to the production of (2*S*)-naringenin in *S. cerevisiae*. Solid lines represent a single step; dotted lines indicate multiple steps; the blue arrows represent the core (2*S*)-naringenin biosynthetic pathway and a variety of plant specific flavonoids derived from (2*S*)-naringenin. *ARO3*, DAHP synthase; *ARO4**, L-tyrosine-feedback-insensitive DAHP synthase (*ARO4*^{K229L}); *ARO1*, pentafunctional aromatic protein; *EcoroL*, shikimate kinase from *E. coli*; *ARO2*, chorismate synthase; *ARO7**, L-tyrosine-feedback insensitive chorismate mutase (*ARO7*^{G141S}); *AtPAL2*, phenylalanine ammonia lyase, *AtC4H*, cinnamic acid hydroxylase and *AtATR2*, cytochrome P450 reductase, from *Arabidopsis thaliana*; *CYB5,* yeast native cytochrome *b*5; 4CL, *p*-coumaroyl-CoA ligase; *CHS*, chalcone synthase; *CHI,* chalcone isomerase. E4P, erythrose-4-phosphate; PEP, phosphoenolpyruvate; DAHP, 3-deoxy-D-arabino-2-heptulosonic acid 7-phosphate; SHIK, shikimate; S3P, shikimate-3-phosphate; EPSP, 5-enolpyruvyl-shikimate-3-phosphate; CHA, chorismic acid; PPA, prephenate; L-Phe, L-phenylalanine; *p*HCA, *p*-coumaric acid; NAG, (2*S*)-naringenin. (B) (2*S*)-naringenin production by engineered strains expressing the core (2*S*)-naringenin biosynthetic genes from different sources. *p*HCA^1 represents *p*-coumaric acid biosynthesis pathway consisting of *AtPAL2*, *AtC4H*, *AtATR2* and *CYB5*. Cultures were sampled after 96 h of growth for total *p*-coumaric acid and (2*S*)-naringenin detection. (C) Metabolic engineering to enhance the metabolic flux from glucose to *p*-coumaric acid. NAG^1 represents the basic core (2*S*)-naringenin biosynthetic pathway, consisting of one copy of *At4CL1* from *A. thaliana*, *RsCHS* from *Rhododendron simsii* and *PsCHI* from *Paeonia suffruticosa*. Cultures were sampled after 96 h of growth for total *p*-coumaric acid and (2*S*)-naringenin detection. (D)(E) The total production and extracellular content of *p*-coumaric acid and (2*S*)-naringenin in different engineered strains. The cells were cultivated in defined minimal medium with 30 g/L glucose as the sole carbon source. Cultures were sampled at different time points for total *p*-coumaric acid and (2*S*)-naringenin detection, and supernatants were sampled for extracellular *p*-coumaric acid and (2*S*)-naringenin quantification. Statistical analysis was carried out by using Student's *t*-test (two-tailed; two-sample unequal variance; $^*P < 0.05$, $^{**}P < 0.01$, $^{***}P < 0.001$). All data represent the mean of n = 3 biologically independent samples and error bars show standard deviation.

plant pathway enzymes into a microbial host the cellular environment for protein folding, modification and localization can be different, which may lead to distinct enzyme activities and intermediate transportation processes. For instance, when plant alkaloid pathways that are distributed across different organelles and tissues were reconstituted in yeast, it showed the production of previously inaccessible intermediates due to the unicellular characteristic of yeast (Li and Smolke, 2016), or limitations in cellular transport of intermediates due to the lack of appropriate transporters (Srinivasan and Smolke, 2021).

In this study, we quantified the intracellular and extracellular content of (2*S*)-naringenin and the intermediate *p*-coumaric acid during the whole culture process. We show that fine-tuning of *p*-coumaric acid synthesis alleviated growth defects and improved (2*S*)-naringenin production in yeast. Furthermore, potential transporters were also exploited to prevent the export of *p*-coumaric acid or enhance the export of (2*S*)-naringenin. Subsequently, a high-level production of (2*S*)-naringenin was achieved, up to 2.05 g/L in minimal medium under fed-batch fermentation conditions. We believe that the strategies developed could be potentially applicable in other microbial systems with the aim for controlling pathway intermediates secretion/accumulation for microbial based production of plant natural products.

2. Results

2.1. Extracellular accumulation of p-coumaric acid limits (2S)-naringenin production

As shown in Fig. 1A, an $_{L}$-phenylalanine-based pathway was used for *de novo* synthesis of *p*-coumaric acid as described earlier (Liu et al., 2019). To further construct the (2*S*)-naringenin biosynthetic pathway, we screened CHSs and CHIs from different sources (Fig. 1B). Among the different combinations of CHSs and CHIs, a strain containing *RsCHS* from *Rhododendron simsii* and *PsCHI* from *Paeonia suffruticosa* was found to be best resulting in production of 35 mg/l of (2*S*)-naringenin. As *p*-coumaric acid is an essential precursor for (2*S*)-naringenin production, we next expressed feedback resistant variants of *ARO4** and *ARO7**, and additional copies of *ARO1/2/3* together with *EcaroL* from *E. coli*, which has been previously shown to significantly improve *p*-coumaric acid production (Liu et al., 2019). This resulted in increased (2*S*)-naringenin production, up to 68 mg/L in strain NAG10 (Fig. 1C). However, further enhancement of *p*-coumaric acid production by additionally expressing *PHA2* led to decreased (2*S*)-naringenin production in NAG11, while at the same time *p*-coumaric acid production increased significantly, up to 350 mg/L (Fig. 1C).

When we examined the whole production process it was found that more than 90% of the *p*-coumaric acid produced was secreted out of the cell independent of production level (Fig. 1D), indicating that yeast cells are very efficient in exporting *p*-coumaric acid. On the other hand, (2*S*)-naringenin seemed to be secreted mainly during the first 24 h and then started to accumulate intracellularly (Fig. 1E). Moreover, the accumulation of *p*-coumaric acid did not show obviously decrease and the production of (2*S*)-naringenin also did not show markedly increase even with prolonged cultivation time to 120 h (Fig. S1). This indicated that extracellular *p*-coumaric acid was not efficiently re-imported by the cells for (2*S*)-naringenin biosynthesis. To further investigate the uptake of extracellular *p*-coumaric acid, strain IMX581N4, only harboring *At4CL*, *RsCHS* and *PsCHI*, was tested by feeding different concentrations of *p*-coumaric acid (100, 200, 300, 400 mg/L) (Fig. S2). As expected, only 34 mg/L (2*S*)-naringenin was produced when 200 mg/L *p*-coumaric acid was added, afterwards the incremental addition of *p*-coumaric acid did not gradually improve the titer of (2*S*)-naringenin and amounts of *p*-coumaric acid started to accumulate outside the cell. Taken together, these results indicated the distribution of *p*-coumaric acid might become a restriction for the *de novo* biosynthesis of (2*S*)-naringenin in yeast.

Comparing strains NAG05, NAG10 and NAG11, which have increasing capabilities of *p*-coumaric acid production, only the intermediate level of *p*-coumaric acid production (NAG10) improved (2*S*)-naringenin production. Nevertheless, still excessive *p*-coumaric acid (204 mg/L) was secreted by NAG10. This could imply that the pathway downstream of *p*-coumaric acid is insufficient and/or the other precursor malonyl-CoA is limiting.

2.2. Alleviating the bottleneck downstream of p-coumaric acid improves (2S)-naringenin production

We first checked if the expression level of downstream enzymes of *p*-coumaric acid limited (2*S*)-naringenin production. Variant gene copies of 4CL, *CHS* and *CHI* were inserted into the genome of the NAG10 strain (Fig. 2A). Overexpressing all three enzymes individually increased (2*S*)-naringenin production, while simultaneous overexpression of *CHS* and *CHI* had a more pronounced effect. We thus grouped *CHS* and *CHI* together and systematically evaluated the effect of overexpression of 4CL and *CHS&CHI* in the range of 1–4 copies (Fig. 2B). Generally, with a fixed 4CL level increasing the expression of *CHS&CHI* from 1 to 4 copies, (2*S*)-naringenin production increased accordingly, strongly suggesting that the activity of these two enzymes was not sufficient. When 4CL increased from 3 to 4 copies, the trend of increasing (2*S*)-naringenin production seemed to be saturated, and further increasing the gene copy number of either 4CL or *CHS&CHI* did not improve (2*S*)-naringenin production anymore (Fig. S3). Eventually, the optimal ratio of 4CL and *CHS&CHI* in NAG3-4 was 3:4, which led to production of 209 mg/L of (2*S*)-naringenin, a 3-fold improvement relative to the parental strain NAG10.

Interestingly, when the copy number of 4CL increased from 1 to 3 there was also a trend towards decreased *p*-coumaric acid accumulation (Fig. 2B), whereas its accumulation was not significantly affected by the expression level of *CHS&CHI*. This could be due to the competition between potential transporter(s) and 4CL for the same substrate of *p*-coumaric acid; if it is not captured by 4CL then it will be secreted out of the cell. Nonetheless, when 4CL increased from 3 to 4 copies, there was no further decrease of *p*-coumaric acid accumulation. These results indicated that the accumulation of *p*-coumaric acid cannot be eliminated completely by expanding the expression level of downstream enzymes.

2.3. Elevated malonyl-CoA supply increases (2S)-naringenin production

Malonyl-CoA is another important precursor for flavonoid biosynthesis, and enhancing malonyl-CoA flux may thus push the biosynthesis pathway to improve (2*S*)-naringenin production while reducing *p*-coumaric acid accumulation. To evaluate the effect of malonyl-CoA supply on (2*S*)-naringenin production, we used three approaches, i) a mutant version of Acc1(catalyzing the formation of malonyl-CoA from acetyl-CoA), mAcc1* (Acc1^{S659A,S1157A}) with enhanced activity (Shi et al., 2014); ii) an alternative pathway from *Rhizobium trifolii* containing a malonate transporter (matC) and activation (matB) for malonyl-CoA formation (Leonard et al., 2008); and iii) a combination of these two methods. We first tested these strategies in the background of the NAG10 strain (Fig. 3A). Expression of either mAcc1* or matBC improved (2*S*)-naringenin production, while the combination of these two strategies gave the highest production at 122 mg/L of (2*S*)-naringenin, representing an 80% increase compared with NAG10. However, the increase was less efficient than the enhanced *p*-coumaric acid downstream pathway, which resulted in 209 mg/L of (2*S*)-naringenin, pointing that the efficiency of the *p*-coumaric acid downstream pathway is more severely limited. Surprisingly, (2*S*)-naringenin production was not significantly increased further when we tested these malonyl-CoA supply strategies in the background of the NAG3-4 strain (Fig. 3B). However, the accumulation of *p*-coumaric acid was further increased when expressing mAcc1* and matBC in both NAG10 and NAG3-4 (Fig. 3A and B). At the same time, the final biomass was significantly decreased especially in the strain with both mAcc1* and matBC, which may indicate an imbalance in the supply of precursor *p*-coumaric acid

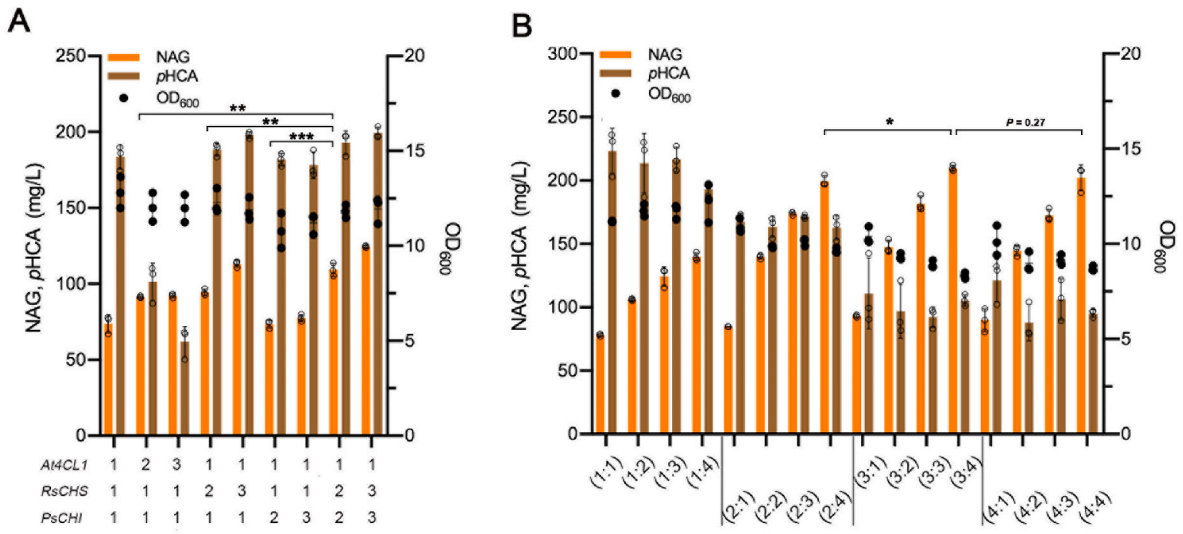

Fig. 2. Optimization of the core (2*S*)-naringenin biosynthetic pathway. (A) Rate-limiting steps were analyzed by gradually increasing the gene copy number of each step. (B) Fine-tuning the expression of 4CL and CHS&CHI to improve (2*S*)-naringenin production. The numbers (n:n) indicate the respective gene copy numbers of 4CL and *CHS&CHI*. Cells were grown in a defined minimal medium with 30 g/L glucose as the sole carbon source, and cultures were sampled after 96 h of growth for total *p*-coumaric acid and (2*S*)-naringenin detection. Statistical analysis was carried out by using Student's *t*-test (two-tailed; two-sample unequal variance; $*P < 0.05$, $**P < 0.01$, $***P < 0.001$). All data represent the mean of n = 3 biologically independent samples and error bars show standard deviation.

and malonyl-CoA.

We further examined these strains in a fed-batch-like condition with slow release of glucose. Here, a more substantial increase was found in both background of NAG10 and NAG3-4 strains (Fig. 3C and D). Expression of either mAcc1* or matBC improved (2*S*)-naringenin production by about 2-fold, while the combination of the two increased (2*S*)-naringenin production by more than 3-fold, up to 223 mg/L (2*S*)-naringenin in strain NAG14. Although in batch conditions there was no titer increase in NAG3-4, a significant increase was observed under fed-batch mimicking conditions. The combination of mAcc1*and matBC resulted in the highest production up to 436 mg/L in NAG39, representing a 2-fold improvement relative to the NAG3-4 background strain. However, this increase was less than that of NAG10 background strain, suggesting that malonyl-CoA still was the limiting factor in NAG39.

To evaluate malonyl-CoA availability, we used a previously reported malonyl-CoA biosensor (David et al., 2016) to quantify the malonyl-CoA supply of three strategies in NAG3-4 background strains. The results revealed that all the methods could significantly increase the level of malonyl-CoA under two different culture conditions (Figs. S4 and S5). Specifically, the fluorescence level in the strain with the combination of mAcc1*and matBC was significantly higher than in the strains with the individual modifications, which was consistent with the increase of (2*S*)-naringenin production.

Compared with the normal batch conditions, the fed-batch like cultivation limits the overflow metabolism through continuously releasing glucose at a low level (Liu et al., 2019). Thus, we inferred that to a certain extent the metabolic flux between the *p*-coumaric acid synthesis and malonyl-CoA supply was balanced under fed-batch mimicking conditions. Although there was no direct evidence yet, this strategy has been effective to several other flavonoid products derived from *p*-coumaric acid and cinnamic acid (flavonoid intermediates similar to *p*-coumaric acid) (Tartik et al., 2023; Tous Mohedano et al., 2023). However, under this condition, *p*-coumaric acid still accumulated and biomass production was significantly reduced in NAG39. Furthermore, we confirmed that the accumulation of *p*-coumaric acid was still mostly extracellular in both culture conditions (Figs. S6 and S7). Therefore, novel strategies are required to address the secretion and accumulation of *p*-coumaric acid for efficient production of (2*S*)-naringenin.

2.4. Dynamic regulation of p-coumaric acid synthesis reduces its accumulation

To address the *p*-coumaric acid accumulation issue, we implemented the aforementioned malonyl-CoA biosensor to dynamically control the production rate of *p*-coumaric acid during cell growth (Fig. 4A). Additionally, in our previous studies, a set of synthetic promoters was developed with varied sensitivity and dynamic ranges in response to malonyl-CoA by changing number and/or inserting position of *fapO* in native yeast promoters (Dabirian et al., 2019). Thus, these modified promoters were chosen to control the expression of *AtPAL*, which is the first enzyme of the pathway leading to *p*-coumaric acid synthesis.

To examine the activity of these modified promoters and the impact of dynamic regulation on (2*S*)-naringenin production, we constructed a series of strains by replacing the promoter of *AtPAL* in NAG39 with the modified promoters (containing fap*O*, a 34 bp binding sequence (BS)) and the corresponding native promoters (without BS). Among the tested promoters, p*GPM1*, p*CCW12*, p*TDH3* and p*TEF1*, led to similar production profiles and final OD even with BS inserted in the promoter region as long as FapR was not present (Fig. 4B). However, when FapR was introduced in these strains, as shown in Fig. 4C, the modified promoters exhibited different impacts on regulation of *p*-coumaric acid formation. With modified *CCW12* promoters containing one or three BS elements (in strain NAG68 and NAG69), low levels of *p*-coumaric acid were detected. However, the (2*S*)-naringenin production of NAG68 and NAG69 was much lower than that of NAG60 and NAG61 strains without FapR expression. Surprisingly, the NAG67 strain containing the native *CCW12* promoter displayed lower (2*S*)-naringenin production than NAG59 in absence of the FapR repressor, indicating that the basal activity of native and modified *CCW12* promoters were affected by the expression of FapR. Nevertheless, this was not the case for *TDH3* and *TEF1* promoters when compared with and without FapR expression. For the modified *TDH3* promoter, the *p*-coumaric acid accumulation in NAG71 was dramatically decreased to 16 mg/L, a 93% reduction compared with NAG70 (219 mg/L) expressing *AtPAL* under the native *TDH3* promoter. However, with the modified *TEF1* promoter in NAG73 the accumulation of *p*-coumaric acid only decreased 3-fold (67 mg/L), relative to the NAG72 control strain (209 mg/L), which may be due to the leaky expression of the modified *TEF1* promoter.

To further evaluate the dynamic regulation system, we analyzed the

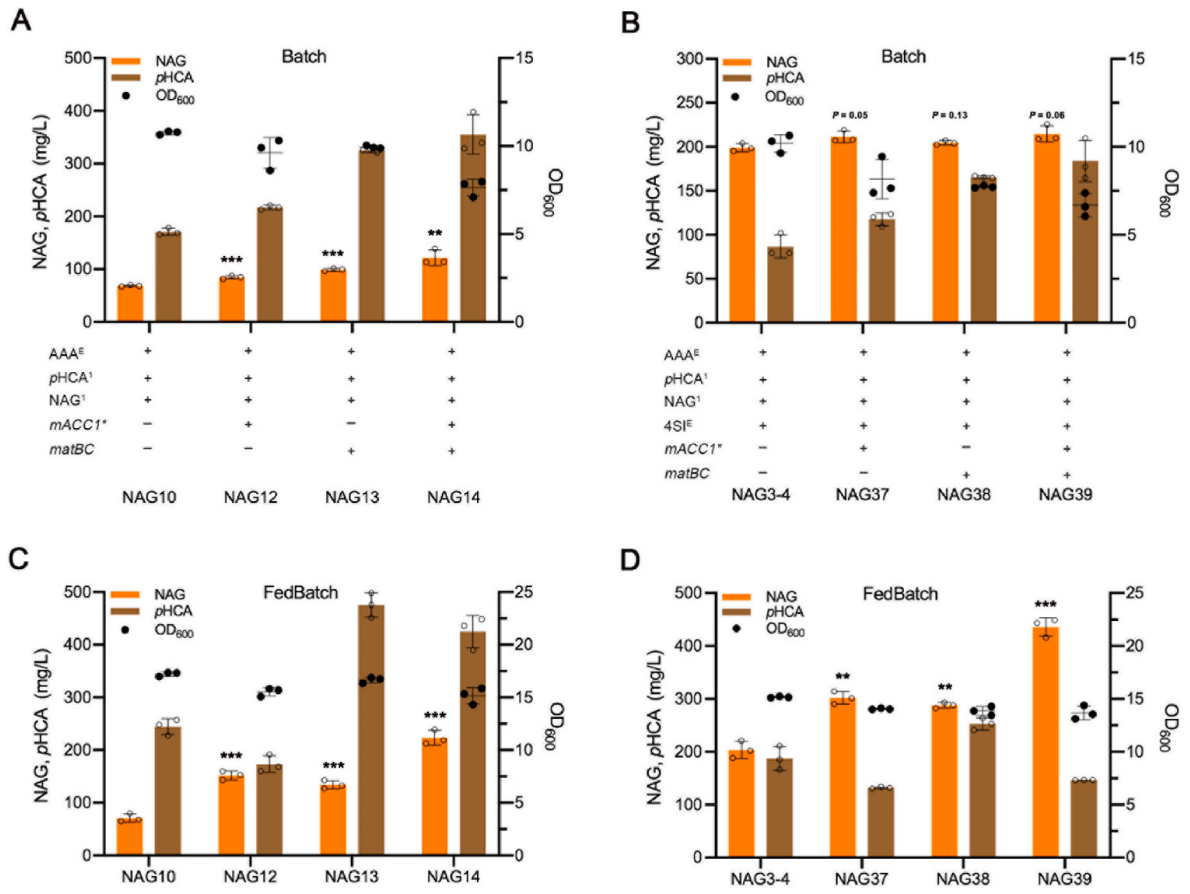

Fig. 3. Improving the malonyl-CoA availability to increase (2*S*)-naringenin production. (A)(B) Production of (2*S*)-naringenin in batch condition by strains with different strategies to enhance the supply of malonyl-CoA. AAA^E represents the overexpression of $_L$-phenylalanine biosynthesis pathway. *p*HCA^1 refers to *p*-coumaric acid biosynthesis pathway. NAG^1 represents the basic core (2*S*)-naringenin biosynthetic pathway, consisting of one copy of *At4CL1* from *A. thaliana*, *RsCHS* from *Rhododendron simsii* and *PsCHI* from *Paeonia suffruticosa*. $4SI^E$ represents the optimization of the core (2*S*)-naringenin biosynthetic pathway, including two copies of *At4CL1*, three copies of *RsCHS* and *PsCHI*. *mACC1** represents the overexpression of $ACC1^{S659A,\ S1157A}$. matB,C represents malonate assimilation pathway. Cells were grown in defined minimal medium with 30 g/L glucose, and with 2 g/L sodium malonate dibasic supplementation when required. Cultures were sampled after 96 h of cultivation for metabolite detection. (C)(D) Fed-batch-like fermentation for (2*S*)-naringenin production by malonyl-CoA enhancing strains derived from NAG10 and NAG3-4 background strains, respectively. Cells were grown in defined minimal medium with six tablets of FeedBeads as the sole carbon source, and with 2 g/L sodium malonate dibasic supplementation when required. Cultures were sampled after 96 h of cultivation for total *p*-coumaric acid and (2*S*)-naringenin detection. Statistical analysis was carried out by using Student's *t*-test (two-tailed; two-sample unequal variance; $^*P < 0.05$, $^{**}P < 0.01$, $^{***}P < 0.001$). All data represent the mean of n = 3 biologically independent samples and error bars show standard deviation.

time course of *p*-coumaric acid production in engineered strains expressing *AtPAL* under different modified promoters with the presence of FapR. As shown, *p*-coumaric acid synthesis was tightly controlled by the modified *TDH3* promoter during the whole culture process (Fig. S8). Overall, these results clearly demonstrated that the dynamic regulation strategy was able to effectively reduce the extracellular accumulation of *p*-coumaric acid, whereas no increase of (2*S*)-naringenin production was found. To validate malonyl-CoA availability in the strains with or without dynamic control, a malonyl-CoA biosensor was introduced in the strains NAG39-2, NAG70, NAG71 and NAG73. Compared with the GFP signals of NAG39-2 and NAG70 without dynamic control, there was no significantly increase of fluorescence in NAG71 and NAG73 (Fig. S9). This indicated that the strains with malonyl-CoA sensor integrated in the genome did not change the concentration of intracellular malonyl-CoA. This result was also consistent with no increase of (2*S*)-naringenin production in the dynamic control strains. Interestingly, when FapR was present, a significant improvement in the final biomass was observed in all the strains with modified promoters (in NAG68, NAG69, NAG71 and NAG73, Fig. 4C), compared with the control strain with corresponding native promoters. This could be explained by the fact that to a certain extent the carbon flux was shifted from *p*-coumaric acid formation towards biomass production. This result inspired us to investigate whether we could further turn the saved carbon, which otherwise led to *p*-coumaric acid accumulation, to the biosynthesis of (2*S*)-naringenin by further balancing *p*-coumaric acid synthesis and malonyl-CoA availability.

2.5. Dynamic regulation of malonyl-CoA diversion increases (2S)-naringenin production

In *S. cerevisiae,* the intracellular malonyl-CoA synthesis is tightly regulated and mainly consumed for synthesizing fatty acids, which are directly associated with cell growth and cell membrane biosynthesis (Tehlivets et al., 2007). To further improve malonyl-CoA availability, we sought to fine-tune the expression of fatty acid synthase through the dynamic control system combined with an RNA interference (RNAi) strategy (Fig. 4A). The fatty acid synthase complex comprises Fas1 and Fas2 subunits, and the *FAS2* gene is autoregulated by the *FAS1* gene product to coordinate the activity of the fatty acid synthase system (Wenz et al., 2001). Therefore, the expression of *FAS1* was put under control of the dynamic RNAi system to divert malonyl-CoA flux from fatty acid synthesis to (2S)-naringenin biosynthesis.

To reconstitute the RNAi mechanism in *S. cerevisiae*, two heterologous genes, *AGO1* and *DCR1* (coding for Argonaute and Dicer,

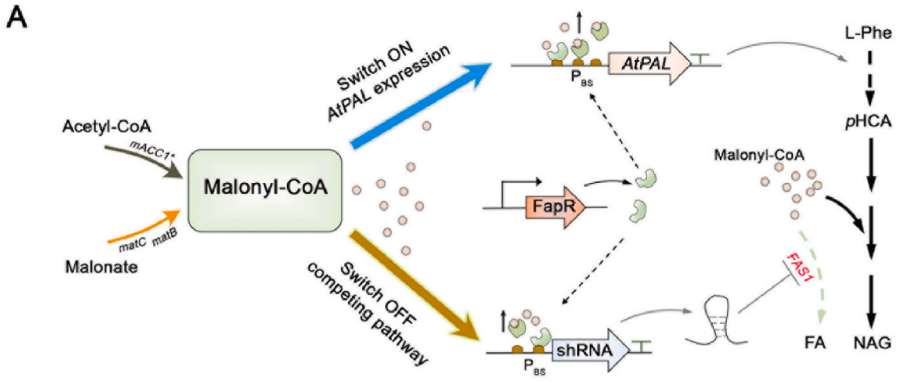

Promoter of *AtPAL*	Strain	
	(-)FapR	(+)FapR
pGPM1	NAG39	NAG39-2
pGPM1	NAG58	NAG66
pCCW12	NAG59	NAG67
pCCW12BS2	NAG60	NAG68
pCCW12_BS123	NAG61	NAG69
pTDH3	NAG62	NAG70
pTDH3_BS23	NAG63	NAG71
pTEF1	NAG64	NAG72
pTEF1_BS123	NAG65	NAG73

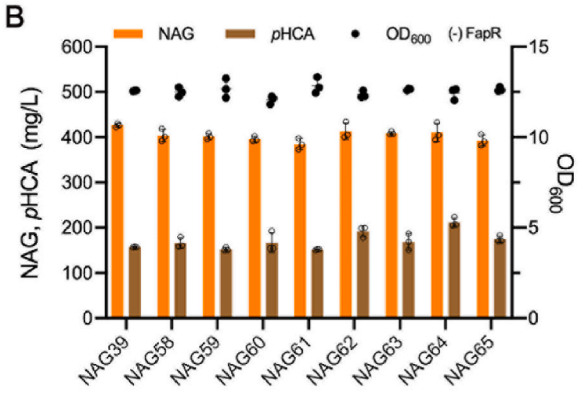

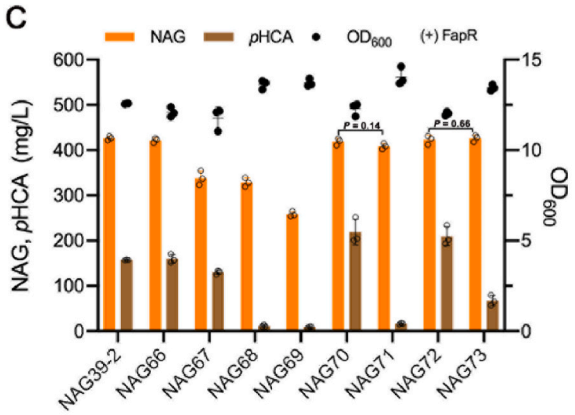

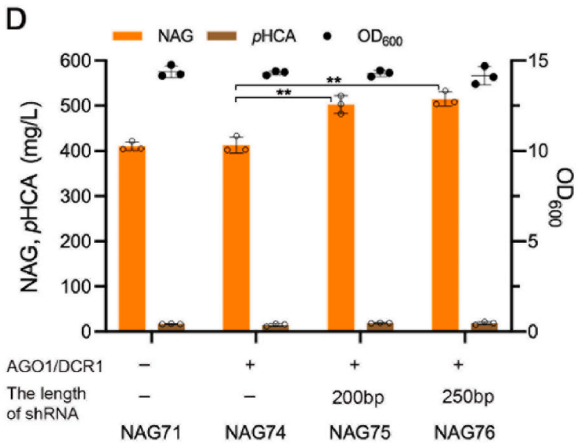

Fig. 4. Construction of a dual dynamic control network to improve (2*S*)-naringenin production. (A) Schematic diagram of the dual dynamic control system for dynamic activation (Switch ON) and repression (Switch OFF) of genes expression. *matC*, malonate carrier protein and *matB*, malonate synthetase from *Rhizobium trifolii*; *mACC1** represents Acc1$^{S659A,\ S1157A}$; *FAS1*, beta subunit of fatty acid synthetase; FA, fatty acid; L-Phe, L-phenylalanine; *p*HCA, *p*-coumaric acid; NAG, (2*S*)-naringenin. (B) Evaluation the effect of different modified promoters to control *p*-coumaric acid production on (2*S*)-naringenin production and *p*-coumaric acid accumulation in the absence of the FapR repressor. The strains with respective native promoters were used as the control. (C) Investigation of the malonyl-CoA sensor for (2*S*)-naringenin pathway regulation. Production of (2*S*)-naringenin and accumulation of *p*-coumaric acid in the strains expressed *AtPAL* under modified promoters and native promoters, were compared in presence of FapR repressor. (D) Dynamic downregulation of *FAS1* expression by RNAi under the control of the modified *TDH3* promoter. In B, C, D for the shake-flask fed-batch conditions, cells were grown in defined minimal medium with six tablets of FeedBeads as the sole carbon source and with 2 g/L sodium malonate dibasic supplementation. Cultures were sampled after 96 h of cultivation for total *p*-coumaric acid and (2*S*)-naringenin detection. Statistical analysis was carried out by using Student's *t*-test (two-tailed; two-sample unequal variance; $*P < 0.05$, $**P < 0.01$, $***P < 0.001$). All data represent the mean of n = 3 biologically independent samples and error bars show standard deviation.

respectively) from *Saccharomyces castellii* (Drinnenberg et al., 2009), were introduced into the genome of the NAG71. Small hairpin RNAs (shRNAs), consisting of both antisense and sense DNA strand of the target gene separated by a hairpin loop, have been reported to be stronger silencing constructs compared with double-stranded RNA generated by expression of antisense-RNA (Kildegaard et al., 2019). Also, the hairpin length was proved to be a factor that affects the efficiency of RNAi (Crook et al., 2014). Hence, two shRNAs of different length, 200 bp and 250 bp, were designed to evaluate the efficiency of the downregulation of *FAS1*. The modified *TDH3* promoter described above, as the most tightly regulated promoter, was selected for the expression of shRNA constructs. Expressing shRNAs under the modified *TDH3* promoter further enhanced the (2*S*)-naringenin production to 502 mg/L and 514 mg/L in NAG75 and NAG76 strains, respectively, a

22% and 25% improvement compared with the control strain NAG74 (Fig. 4D). Additionally, NAG75 and NAG76 showed a final biomass similar to the NAG74 and NAG71 strains. When the shRNAs were expressed under the native *TDH3* promoter as control, all the transformants showed the formation of tiny colonies and grew very slowly, suggesting that constitutive expression of shRNAs to silence fatty acid synthesis may be detrimental for growth. Meanwhile, the concentration of malonyl-CoA in the NAG75 and NAG76 strains was quantified by using a malonyl-CoA biosensor. The results showed that the fluorescence was increased in NAG75 and NAG76 strains when comparing to the GFP signal of NAG74 (Fig. S10). Overall, as a proof-of-concept, the dynamic RNAi system was proved to be functional and was able to improve (2*S*)-naringenin production.

2.6. Exploitation of potential transporters increases (2S)-naringenin production

In parallel to the dual dynamic control system, transporter engineering could be an effective approach to reduce the export and thus the extracellular accumulation of *p*-coumaric acid or to enhance the export of (2*S*)-naringenin to increase flux through the (2*S*)-naringenin production pathway. To validate this feasibility, several candidate transporters were evaluated. Specifically, two transporters (*TAT1* and *TPO1*) involved in the transport of amino acids (Rodriguez et al., 2017), two transporters (*ESBP6* and *PDR12*) found to be responsible for increasing tolerance to aromatic acids (Pereira et al., 2020), and one transcriptional factor (*PDR1*) regulating multiple ABC transporter genes such as *SNQ2*, *PDR5*, *PDR11* and *YOR1* were investigated. The latter transporter genes display high similarity to the transporter gene *MtABCG10* from *Medicago truncatula* involved in the membrane translocation of *p*-coumaric acid (Biala et al., 2017; Jungwirth and Kuchler, 2006).

We firstly compared overexpression and deletion of the selected targets in NAG10 (Fig. 5A, Fig. S11). Overexpression of *ESBP6* and *PDR12* led to reduced accumulation of *p*-coumaric acid, indicating these two may be related to the transport of *p*-coumaric acid. However, only *PDR12* overexpression showed an increase of (2*S*)-naringenin production by 13.5% (Fig. 5A). To validate the potential of candidate transporters for *p*-coumaric acid uptake, extracellularly feeding *p*-coumaric acid as substrate was conducted in an IMX581N4 background (Fig. 5B, Fig. S12). As shown before, when 300 mg/L *p*-coumaric acid was added to IMX581N4, about one third of *p*-coumaric acid left and mostly accumulated outside of the cell (Fig. S2). Both *ESBP6* and *PDR12* overexpression significantly decreased the accumulation of *p*-coumaric acid, while only overexpression of *PDR12* exhibited a 1.6-fold increase in (2*S*)-naringenin production, compared with the control IMX581N4 strain. Surprisingly, overexpression of *ESBP6* in IMX581N4 led to reduction in *p*-coumaric acid accumulation, indicating the potential function of importing this compound. This contradicted previous reports on Esbp6 exporting this compound under low pH condition (Pereira et al., 2020). Therefore, we compared the accumulation of *p*-coumaric acid in these strains at pH 6.0 and 3.5 (Fig. S13). At pH 3.5, a clear increase of *p*-coumaric acid accumulation was seen for both NAG10 and IMX581N4 backgrounds, while it was reversed at pH 6.0, which indicates the effect of pH on the function of Esbp6.

Thus, we focused on *PDR12* by overexpressing it in NAG39 and NAG41 strains, which have a higher flux of the downstream pathway of *p*-coumaric acid compared to NAG10 and IMX581N4. Unexpectedly, the extracellular accumulation of *p*-coumaric acid decreased only slightly while the total (2*S*)-naringenin production were still significantly improved by 17.3% and 28.4% in NAG97 and NAG98, respectively (Fig. 5C). This indicated the possibility that Pdr12 may be related to the transport of (2*S*)-naringenin rather than *p*-coumaric acid. Interestingly, overexpression of *PDR12* increased slightly the extracellular (2*S*)-naringenin by 5% and 8% in NAG97 and NAG98, respectively compared with the control strains NAG39 and NAG41 (Fig. S14). A more efficient export of the product (2*S*)-naringenin would pull the flux through the downstream pathway of *p*-coumaric acid and thus reduce the accumulation of *p*-coumaric acid. Subsequently, *PDR12* was further overexpressed in the dual dynamic control strain NAG76 and evaluated under fed-batch mimicking conditions. With the similar trend, the production of (2*S*)-naringenin was also slightly increased to 563 mg/L in the resultant strain NAG99, representing an additional 9.5% improvement

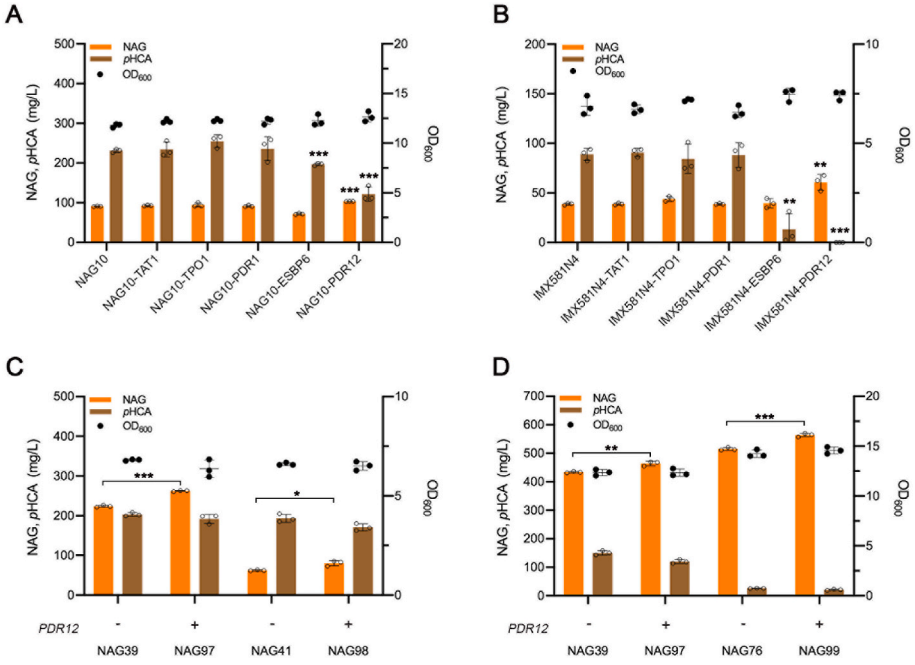

Fig. 5. Evaluation of potential transport and regulator genes on *p*-coumaric acid accumulation and (2*S*)-naringenin production. (A) Effects of target genes overexpression on *p*-coumaric acid accumulation and (2S)-naringenin production in NAG10 strains. The cells were cultivated in defined minimal medium with 30 g/L glucose as the sole carbon source. (B) Uptake of *p*-coumaric acid by overexpressing target genes in IM581N4 background strains. Cells were grown in a defined minimal medium with 30 g/L glucose as the sole carbon source and supplemented with *p*-coumaric acid (300 mg/L) as precursor. (C) Effect of *PDR12* transporter overexpression on *p*-coumaric acid accumulation and (2*S*)-naringenin production under normal batch conditions. Strain NAG39 and NAG97 were grown in defined minimal medium with 30 g/L glucose as the sole carbon source and with 2 g/L sodium malonate dibasic supplementation, while strain NAG41 and NAG98 additionally supplemented with 300 mg/L *p*-coumaric acid. (D) Effect of *PDR12* transporter overexpression on *p*-coumaric acid accumulation and (2*S*)-naringenin production in fed-batch-like conditions. Cells were grown in defined minimal medium with six tablets of FeedBeads as the sole carbon source and with 2 g/L sodium malonate dibasic supplementation. Cultures were sampled after 96 h of cultivation for total *p*-coumaric acid and (2*S*)-naringenin detection. Statistical analysis was carried out by using Student's *t*-test (two-tailed; two-sample unequal variance; $^*P < 0.05$, $^{**}P < 0.01$, $^{***}P < 0.001$). All data represent the mean of n = 3 biologically independent samples and error bars show standard deviation.

relative to strain NAG76 (Fig. 5D). Taking together, Overexpression of *PDR12* can reduce the accumulation of *p*-coumaric acid and increase the production of (2*S*)-naringenin, but the detailed mechanisms require further analysis in the future.

2.7. Fed-batch fermentation enhances (2S)-naringenin production

To evaluate the scalability of the dual dynamic control system, NAG39, NAG76 and NAG99 were cultivated in bioreactors with minimal medium under glucose-limited fed-batch conditions. When glucose and ethanol were depleted, the glucose feeding was initiated (Fig. 6). The titer of (2*S*)-naringenin and biomass rapidly increased in an almost coupled way during the feeding process. In contrast to the control strain NAG39 without dynamic control of *p*-coumaric acid synthesis, the accumulation of *p*-coumaric acid was constantly maintained at a very low level in both NAG76 and NAG99, indicating that the dual dynamic control system could well balance the supply of two precursors and reduce the secretion of *p*-coumaric acid. Furthermore, reaching a certain concentration of *p*-coumaric acid seemed to have a detrimental effect on cell growth, as the biomass level did not increase after the *p*-coumaric acid titer had reached 692.2 mg/L in NAG39 (Fig. 6A).

The total (2*S*)-naringenin production was continuously increased in NAG76 and NAG99, while the secretion of (2*S*)-naringenin in NAG99 was slightly higher than that of NAG76, with 20.2% extracellular (2*S*)-naringenin in NAG99 compared to 15.3% in NAG76 (Fig. 6B and C). Finally, the highest titer of (2*S*)-naringenin reached 1.77 g/L and 2.05 g/L in NAG76 and NAG99 at 120 h, a yield of 16.0 mg/g glucose and 19.2 mg/g glucose, respectively. Compared to the control strain NAG39 without a dynamic control system, these represented a 52% and 76% increase in (2*S*)-naringenin titers, highlighting the importance of controlling secretion/accumulation of pathway intermediates and products.

3. Discussion

(2*S*)-Naringenin is a starting compound for synthesis of a variety of phenylpropanoid and flavonoid chemicals but also possesses many high-value pharmaceutical and nutraceutical properties. In the past decades, significant achievements have been made in microbial synthesis of (2*S*)-naringenin. Different strategies have been implemented to improve (2*S*)-naringenin production, however, fewer studies have focused on the spatiotemporal distribution of (2*S*)-naringenin and its intermediate *p*-coumaric acid. Here, we monitored the intracellular and extracellular content of (2*S*)-naringenin and *p*-coumaric acid over the culture process. We thus established a dual dynamic control system through autonomously controlling the synthesis of *p*-coumaric acid to efficiently reduce its accumulation and downregulating a native pathway competing for malonyl-CoA to simultaneously improve (2*S*)-naringenin production.

The accumulation of *p*-coumaric acid has been observed before in *S. cerevisiae* (Koopman et al., 2012) and *E. coli* (Wu et al., 2014; Zhou et al., 2021) when expressing flavonoid/naringenin biosynthetic pathways. The hypothesis was that reactions downstream of *p*-coumaric acid and/or malonyl-CoA supply was a limiting factor for (2*S*)-naringenin production. Indeed, alleviating the bottleneck downstream of *p*-coumaric acid and increasing malonyl-CoA supply both could further enhance (2*S*)-naringenin production, resulting in less *p*-coumaric acid accumulation. However, significant amounts of *p*-coumaric acid were left even at the end of fermentation (Figs. 2 and 3). One may argue that if the flux towards *p*-coumaric acid should be kept low to avoid this. However, to ultimately increase production of (2*S*)-naringenin and derived products, it is necessary to have a high flux to its precursors. As demonstrated in Fig. 1C, increasing *p*-coumaric acid formation was able to improve (2*S*)-naringenin production.

Alternatively, the transiently accumulated *p*-coumaric acid could be potentially re-consumed later in the fermentation. This had been reported to be the case, but more than one third of formed *p*-coumaric acid was not consumed at the end of fermentation (Koopman et al., 2012), representing a waste of carbon. In addition, accumulation of *p*-coumaric acid could be toxic to microbial cells, as evidenced during the fed-batch fermentation of NAG39 (Fig. 6A). It had been observed to inhibit the growth of *S. cerevisiae* (Pereira et al., 2020), pointing to a necessity of minimizing *p*-coumaric acid accumulation. On the other hand, re-consumption of formed *p*-coumaric acid may be hampered by inefficient import of this compound, as shown by an engineered stain IMX581N4, in which the *p*-coumaric acid conversion rate was only about 10% by exogenous supplementation of *p*-coumaric acid (Fig. S2). This agreed well with earlier reports, where upon supplementation of *p*-coumaric acid as substrate, the conversion yield to (2*S*)-naringenin production only reached between 5.7% and 27.41% in *S. cerevisiae* (Gao et al., 2020b; Trantas et al., 2009; Yan et al., 2005). The low efficiency of *p*-coumaric acid conversion maybe due to the low pathway capacity downstream of *p*-coumaric acid and limiting malonyl-CoA supply. However, the yield was not increased even in a new background strain NAG41 where the downstream *p*-coumaric acid pathway was enhanced and malonyl-CoA supply was elevated (Fig. S15). With more *p*-coumaric acid supplemented, there was a slight trend of increase in the total consumption. Similarly, *p*-coumaric acid started to be accumulated when more than 200 mg/L was fed. This is plausible especially for NAG41, as the highest (2*S*)-naringenin production reached with addition of *p*-coumaric acid was around 76 mg/L in NAG41, about one third of the corresponding strain NAG39 (214 mg/L), where the sole difference was the provision of either exogenous or endogenous *p*-coumaric acid. These results indicate the potential issue with import of *p*-coumaric acid into yeast and highlight the importance of controlling synthesis of *p*-coumaric acid in a *de novo* production strain.

The beneficial effect of the fed-batch model inspired us to consider dynamic control of metabolic flux as a strategy for reducing the accumulation of *p*-coumaric acid and improving (2*S*)-naringenin production. Considering that malonyl-CoA is more severely limited than *p*-coumaric acid, we implemented a malonyl-CoA biosensor to couple *p*-coumaric acid synthesis to cellular malonyl-CoA level (Fig. 4C). To channel more carbon flux toward (2*S*)-naringenin synthesis we further combined this malonyl-CoA sensor with an RNAi strategy to control fatty acid

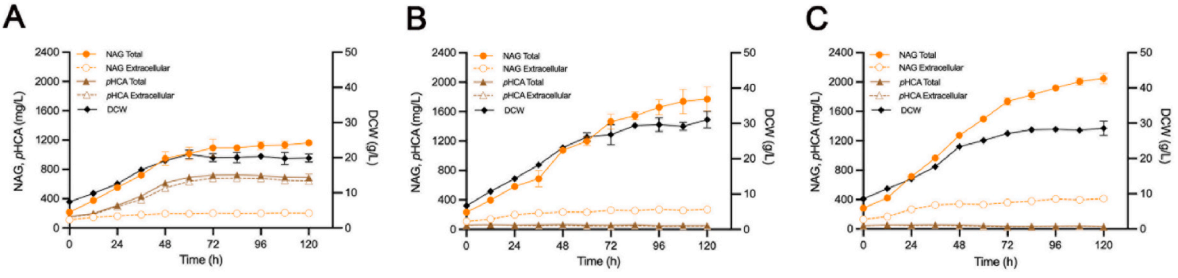

Fig. 6. Fed-batch fermentation profiles of NAG39 (A), NAG76 (B) and NAG99 (C) under glucose-limited conditions. The biomass, total production of (2*S*)-naringenin and *p*-coumaric acid accumulation, and extracellular concentration of (2*S*)-naringenin and *p*-coumaric acid were monitored during the fed-batch cultivation. All data represent the mean of n = 2 biologically independent samples and error bats show standard deviation.

biosynthesis. This dual dynamic system finally increased (2*S*)-naringenin by 25%, without significant accumulation of *p*-coumaric acid and any effect on cell growth (Fig. 4D). Recently, a multi-layered dynamic regulation network was reported to successfully improve (2*S*)-naringenin production with a concomitant increase in cell growth compared to the strain using static strain engineering approach in *E. coli* (Zhou et al., 2021). However, this system requires the presence of intracellular (2*S*)-naringenin and *p*-coumaric acid, which limits its application in other organisms like *S. cerevisiae* and prevents complete removal of *p*-coumaric acid accumulation.

Compared with dynamic control strategies, transport engineering is a more direct approach to deal with the secretion/accumulation of *p*-coumaric acid and improve the yield of (2*S*)-naringenin. However, it would be challenging to identify and control transporters if multiple potential exporters exist, and complex mechanisms are involved transporters activity. As demonstrated by the effect of Esbp6 on *p*-coumaric acid accumulation under different pH conditions (Fig. S13), this further complicates the approach of regulating potential transporters to control the secretion of *p*-coumaric acid. Although Pdr12 has been indicated as a transporter for weak organic acids and aromatic acids, the export of (2*S*)-naringenin or flavonoids has not been reported. The precise function of Pdr12 in *p*-coumaric acid and (2*S*)-naringenin transportation remains to be elucidated in the future.

Finally, a (2*S*)-naringenin titer of 2.05 g/L was achieved in a fed batch fermentation with a yield of 19.2 mg/g glucose (Fig. 6B). Although further optimization is needed, we believe that the platform presented here could be exploited for producing many other important flavonoids. Furthermore, the methods developed in this study to control the synthesis of pathway intermediates could be relevant for other microbial cell factories for producing plant natural products such as flavonoids and alkaloids.

4. Materials and methods

4.1. Strains and reagents

All the *S. cerevisiae* strains and plasmids used in this work are listed in Supplementary Tables 1 and 2. High-fidelity Phusion DNA polymerase was purchased from New England Biolabs. PrimeStar DNA polymerase and SapphireAmp* Fast PCR Master Mix were purchased from TaKaRa Bio. Plasmid extraction and DNA gel purification kits were purchased from ThermoFisher Scientific. All oligonucleotides were synthesized at Integrated DNA Technologies (IDT) and are listed in Supplementary Table 3. All codon-optimized heterologous genes were synthesized at GenScript and are listed in Supplementary Table 4. All chemicals including analytical standards were purchased from Sigma-Aldrich.

4.2. Strain cultivation

S. cerevisiae strains for preparation of competent cells were cultivated in YPD medium consisting of 10 g/L yeast extract (Merck Millipore), 20 g/L peptone (Difco) and 20 g/L glucose (Merck Millipore). Synthetic complete medium without uracil (SC-URA), which consisted of 6.7 g/L yeast nitrogen base without amino acids (Formedium), 0.77 g/L CSM without uracil (Formedium), 20 g/L glucose (Merck Millipore) and 20 g/L agar (Merck Millipore), was used for selection of yeast transformants containing *URA3* marker-based plasmids. To remove the *URA3* maker, yeast transformants were selected against on synthetic complete medium with 5-fluoroorotic acid plates (SC+5-FOA), which contained 6.7 g/L yeast nitrogen base, 0.77 g/L CSM and 0.8 g/L 5-FOA.

Shake flask batch fermentations for the production of (2*S*)-naringenin and *p*-coumaric acid were carried out in minimal medium, containing 7.5 g/L $(NH_4)_2SO_4$, 14.4 g/L KH_2PO_4, 0.5 g/L $MgSO_4{\cdot}7H_2O$, and 30 g/L glucose, 2 mL/L trace metal (3.0 g/L $FeSO_4{\cdot}7H_2O$, 4.5 g/L $ZnSO_4{\cdot}7H_2O$, 4.5 g/L $CaCl_2{\cdot}2H_2O$, 0.84 g/L $MnCl_2{\cdot}2H_2O$, 0.3 g/L $CoCl_2{\cdot}6H_2O$, 0.3 g/L $CuSO_4{\cdot}5H_2O$, 0.4 g/L $Na_2MoO_4{\cdot}2H_2O$, 1.0 g/L H_3BO_3, 0.1 g/L KI, and 19.0 g/L $Na_2EDTA{\cdot}2H_2O$), and 1 mL/L vitamin solutions (0.05 g/L D-biotin, 1.0 g/L D-pantothenic acid hemicalcium salt, 1.0 g/L thiamin–HCl, 1.0 g/L pyridoxin–HCl, 1.0 g/L nicotinic acid, 0.2 g/L 4-aminobenzoic acid, and 25.0 g/L myo-inositol) supplemented with 60 mg/L uracil if needed. Three biological replicates of each engineered strain were inoculated in tubes with 2 mL minimal medium at 30 °C with 220 rpm agitation for 24 h. Then, the precultures were inoculated to the initial OD600 of 0.05 in 15 mL minimal medium or minimal medium containing 2 g/L sodium malonate dibasic (Sigma-Aldrich) in 100 mL unbaffled shake-flasks. The cells were cultured at 30 °C with 220 rpm agitation for 96 h. For shake flask fermentation in mimicked fed-batch condition, six tablets of FeedBeads (SMFB08001, Kuhner Shaker, Basel, Switzerland), corresponding to 30 g/L glucose, were used as the sole carbon source and cultivations were run for 96 h at 30 °C with 220 rpm agitation.

The fed-batch bioreactor fermentation was performed in biological quadruplicates in 1 L bioreactors (DasGip Parallel Bioreactor System, DasGip, Germany) containing 250 mL initial minimal medium with 30 g/L glucose. The temperature (30 °C), pH, agitation and aeration were monitored and controlled using a DasGip Control 4.0 System. The dissolved oxygen level was maintained above 30%. The pH was set at 5.6 and controlled by the addition of 4 M KOH and 2 M HCl. The agitation and aeration were initially set to 600 rpm and 36 L/h respectively. When the dissolved oxygen in the reactor decreased below 30%, the agitation increased to 1000 rpms and the airflow to 48 L/h. The aeration was controlled and provided by a DasGip MX4/4 module. The composition of the off-gas was monitored using a DasGip Off Gas Analyzer GA4. Addition of the acid, base, and glucose feeding was conducted with DasGip MP8 multi-pump modules (pump head tubing: 0.5 mm ID, 1.0 mm wall thickness). During the fed-batch cultivation, the cells were fed a 200 g/L glucose solution with a feeding rate that was exponentially increased ($\mu = 0.05\ h^{-1}$) to maintain a constant growth rate. The used minimal medium contained: 15 g/L $(NH_4)_2SO_4$, 9 g/L KH_2PO_4, 1.5 g/L $MgSO_4{\cdot}7H_2O$, 180 mg/L uracil, 3 ml/L trace metal, 3 ml/L vitamin solutions and 9 g/L sodium malonate dibasic. The initial feeding rate was calculated by using the biomass yield and concentration that were obtained during prior duplicate batch cultivations with this strain. The feeding was initiated after the CO_2 levels dropped indicating that glucose and ethanol were totally consumed. Cell dry weight (CDW) measurements were performed by filtrating 1 mL of cell culture through a weighed 0.45 μm filter membrane (Sartorius Biolab, Gottingen, Germany) and weighting the filter after microwaving it for 15 min and letting it dry in a desiccator for 24 h.

4.3. DNA manipulation

The *S. cerevisiae* CEN.PK113-5D-detivative IMX581 (*MATa ura3-52 can1Δ::cas9-natNT2 TRP1 LEU2 HIS3*) (Mans et al., 2015) was used as original strain for all engineering work. CRISPR–Cas9-mediated genome engineering was used for chromosome-based gene overexpression and the integration of expression cassettes. IMX581 genomic DNA served as the template for all native promoters, genes and terminators. For optimized heterologous genes, synthetic fragments or plasmids were utilized as the DNA template for amplification. High-fidelity Phusion DNA polymerase was used for entire DNA fragment amplifications, except PrimeSTAR HS polymerase was selected for *in vitro* fusion PCR for generating integration modules. Functional expression modules were generated according to the overlapping extension PCR procedure (Zhou et al., 2012), and all used integration modules are listed in Supplementary Table 5.

Specific chromosomal loci (Mikkelsen et al., 2012), enabling stable and high-level expression of heterologous genes, were selected as the recombination sites for integration of gene overexpression modules. Taking construction of NAG05 as an example to show the CRISPR/Cas9-mediated integration of in-vitro-assembled gene expression modules, the integration module was divided into two fragments:

M1 (*XII-4 up-TDH3p-At4CL1-ADH1t* + *TDH2t*) and M6 (*ADH1t* + *TDH2t-RsCHS-CCW12p* + *tHXT7p-PsCHI-FBAt- XII-4 dn*). M1 was generated by fusing DNA parts including *XII-4 up, TDH3p, At4CL, ADH1t, TDH2t*. Specifically, the upstream homologous arm *XII-4 up* (P001, P002), promoters *TDH3p* (P045, P046), terminators *ADH1t* (P047, P048) and *TDH2t* (P049, P050) were amplified from IMX581 genomic DNA, respectively; codon-optimized gene *At4CL1* (P164, P165) was amplified from pCfB0854. M6 was assembled by fusing the DNA parts of *ADH1t, TDH2t, RsCHS, CCW12p, tHXT7p, PsCHI, FBAt* and *XII-4 dn*. Codon-optimized genes *RsCHS* (P166, P167) and *PsCHI* (P168, P169) were amplified by using the synthetic genes as template. Promoters *CCW12p* (P051, P052) and *tHXT7p* (P053, P054), terminator *FBAt* (P055, P056) and the downstream homologous arm *XII-4 dn* (P003, P004) were amplified from IMX581 genomic DNA, respectively. Then, the equimolar amounts of purified fragments M1 and M6 (50–100 ng/kb) with gRNA plasmid pQC010 were co-transformed into the IMX581 strain by using the lithium acetate-mediated yeast transformation protocol (Mans et al., 2015) and transformants selected on SC-URA plates. The grown clones were verified by colony PCR by using SapphireAmp® Fast PCR Master Mix. Subsequently, the correct transformants were streaked on SC+5-FOA plates to loop out the gRNA plasmid and recycle the *URA3* marker.

The *FAS1* hairpin part was constructed according to a described method (Kildegaard et al., 2019), the expression module was divided into two DNA fragments: the sense region was assembled by fusing the DNA parts of upstream homologous fragments of the chromosomal target site, promoter, 250-bp sense sequence of the target gene and the 80-bp sequence spanning intron 1 from *Schizosaccharomyces pombe rad9* representing a hairpin loop. The antisense region was generated through assembling the DNA parts of the 80-bp sequence of intron 1 from *S. pombe rad9*, the antisense region of the target gene (reverse complement of sense region), terminator and downstream homologous fragments of the chromosomal target site. Subsequently, the two fragments were co-transformed and assembled into the genomic integration site via *in vivo* homologous recombination. The correct transformants were then confirmed by colony PCR amplification.

To construct specific guide RNAs for a selected gene/genomic locus, all potential gRNAs were selected and compared with all potential off-targets in the whole CEN.PK113-7D genome using the CRISPRdirect webtool (http://crispr.dbcls.jp/) (Naito et al., 2015). The gRNA plasmids were constructed according to the Gibson assembly method in which gRNA sequence-containing DNA parts were *in vitro* recombined with a vector backbone (Mans et al., 2015). The correct recombinant plasmids were verified by *E. coli* colony PCR and further confirmed by DNA sequencing.

4.4. Metabolite extraction and quantification

For total production analysis of (2*S*)-naringenin and *p*-coumaric acid, 0.5 mL of the culture samples were thoroughly mixed with an equal volume of absolute ethanol (100% v/v) and centrifuged at 12,000 rpm for 10 min. The supernatants were then collected and stored in −20 °C until HPLC detection. To measure the supernatant concentrations of (2*S*)-naringenin and *p*-coumaric acid, a 1.0 mL culture sample was centrifuged at 12,000 rpm for 10 min and filtered through 0.45 μm syringe filter. The filtered supernatants were then saved for HPLC analysis.

Samples were quantified on a Dionex Ultimate 3000 HPLC (Thermo Fisher Scientific, Waltham, MA, USA) equipped with a Discovery HS F5 150 mm × 46 mm column (particle size 5 μm) (Sigma-Aldrich, St. Louis, MO, USA). The column was kept at 30 °C, and metabolites from 10 μL of supernatants were separated. The HPLC analysis was carried out with 10 mM ammonium formate (pH 3.0, adjusted by formic acid) (Solvent A) and acetonitrile (Solvent B) as the eluents. The eluent flow rate was 1.5 mL/min. The gradient program started with 5% of solvent B (0–0.5 min), increased linearly from 5% to 60% (0.5–9.5 min), then the second linear increase from 60% to 100% (9.5–10.5 min) and maintained at 100% for 0.5 min (10.5–11 min), at last a linear decrease from 100% to 5% (11–11.5 min) and maintained at 5% for 1.5 min (11.5–13 min). *p*-Coumaric acid was detected by absorbance at 304 nm with a retention time of 6.3 min (2*S*)-naringenin was detected by absorbance at 289 nm with a retention time of 8.9 min. The (2*S*)-naringenin and *p*-coumaric acid concentrations were calculated from standard curves.

For residual glucose and ethanol detection during fed-batch fermentation in bioreactor, the collected culture samples were centrifuged at 12,000 rpm for 10 min and filtered through 0.45 μm syringe filter. The supernatants were then quantified by HPLC (Thermo Fisher Scientific, CA, USA) equipped with an Aminex HPX-87G column (Bio-Rad, Hercules, CA, USA) and a UV and RI detector. 5 mM H_2SO_4 was used as the mobile phase and the column was kept at 45 °C with a flow rate of 0.6 mL/min for 35 min. The glucose concentrations were calculated from the standard curves.

CRediT authorship contribution statement

Jiwei Mao: Conceptualization, Methodology, Investigation, Visualization, Writing- original draft. Marta Tous Mohedano: Investigation, Formal analysis, Writing-review and editing. Jing Fu: Investigation, Writing-review and editing. Xiaowei Li: Investigation, Writing-review and editing. Quanli Liu: Investigation, Writing-review and editing. Jens Nielsen: Supervision, Resources, Writing-review and editing. Verena Siewers: Supervision, Resources, Writing-review and editing. Yun Chen: Conceptualization, Supervision, Resources, Funding acquisition, Writing-review and editing.

Declaration of competing interest

The authors declare no competing interests.

Data availability

Data will be made available on request.

Acknowledgments

We acknowledge funding from the European Union's Horizon 2020 research and innovation program under Grant Agreement No. 686070, the Novo Nordisk Foundation (grant no. NNF10CC1016517 and NNF18OC0034844). We also acknowledge funding support from Vetenskapsrådet and Stiftelsen för internationalisering av högre utbildning och forskning.

Appendix A. Supplementary data

Supplementary data to this article can be found online at https://doi.org/10.1016/j.ymben.2023.08.003.

References

Biala, W., Banasiak, J., Jarzyniak, K., Pawela, A., Jasinski, M., 2017. *Medicago truncatula* ABCG10 is a transporter of 4-coumarate and liquiritigenin in the medicarpin biosynthetic pathway. J. Exp. Bot. 68, 3231–3241.

Birt, D.F., Hendrich, S., Wang, W., 2001. Dietary agents in cancer prevention: flavonoids and isoflavonoids. Pharmacol. Ther. 90, 157–177.

Clementi, N., Scagnolari, C., D'Amore, A., Palombi, F., Criscuolo, E., Frasca, F., Pierangeli, A., Mancini, N., Antonelli, G., Clementi, M., Carpaneto, A., Filippini, A., 2021. Naringenin is a powerful inhibitor of SARS-CoV-2 infection in vitro. Pharmacol. Res. 163, 105255.

Crook, N.C., Schmitz, A.C., Alper, H.S., 2014. Optimization of a yeast RNA interference system for controlling gene expression and enabling rapid metabolic engineering. ACS Synth. Biol. 3, 307–313.

Dabirian, Y., Li, X., Chen, Y., David, F., Nielsen, J., Siewers, V., 2019. Expanding the dynamic range of a transcription factor-based biosensor in *Saccharomyces cerevisiae*. ACS Synth. Biol. 8, 1968–1975.

David, F., Nielsen, J., Siewers, V., 2016. Flux control at the malonyl-CoA node through hierarchical dynamic pathway regulation in *Saccharomyces cerevisiae*. ACS Synth. Biol. 5, 224–233.

Dinh, C.V., Chen, X., Prather, K.L.J., 2020. Development of a quorum-sensing based circuit for control of coculture population composition in a naringenin production system. ACS Synth. Biol. 9, 590–597.
Dinh, C.V., Prather, K.L.J., 2019. Development of an autonomous and bifunctional quorum-sensing circuit for metabolic flux control in engineered *Escherichia coli*. Proc. Natl. Acad. Sci. U.S.A. 116, 25562–25568.
Drinnenberg, I.A., Weinberg, D.E., Xie, K.T., Mower, J.P., Wolfe, K.H., Fink, G.R., Bartel, D.P., 2009. RNAi in budding yeast. Science 326, 544–550.
Dunstan, M.S., Robinson, C.J., Jervis, A.J., Yan, C., Carbonell, P., Hollywood, K.A., Currin, A., Swainston, N., Feuvre, R.L., Micklefield, J., Faulon, J.L., Breitling, R., Turner, N., Takano, E., Scrutton, N.S., 2020. Engineering *Escherichia coli* towards *de novo* production of gatekeeper (2*S*)-flavanones: naringenin, pinocembrin, eriodictyol and homoeriodictyol. Synth Biol (Oxf). 5 ysaa012.
Gao, S., Lyu, Y., Zeng, W., Du, G., Zhou, J., Chen, J., 2020a. Efficient biosynthesis of (2*S*)-naringenin from *p*-coumaric acid in *Saccharomyces cerevisiae*. J. Agric. Food Chem. 68, 1015–1021.
Gao, S., Zhou, H., Zhou, J., Chen, J., 2020b. Promoter-library-based pathway optimization for efficient (2*S*)-naringenin production from *p*-coumaric acid in *Saccharomyces cerevisiae*. J. Agric. Food Chem. 68, 6884–6891.
Hwang, H.G., Noh, M.H., Koffas, M.A.G., Jang, S., Jung, G.Y., 2021. Multi-level rebalancing of the naringenin pathway using riboswitch-guided high-throughput screening. Metab. Eng. 67, 417–427.
Jamil, O.K., Cravens, A., Payne, J.T., Kim, C.Y., Smolke, C.D., 2022. Biosynthesis of tetrahydropapaverine and semisynthesis of papaverine in yeast. Proc. Natl. Acad. Sci. U.S.A. 119, e2205848119.
Jungwirth, H., Kuchler, K., 2006. Yeast ABC transporters– a tale of sex, stress, drugs and aging. FEBS Lett. 580, 1131–1138.
Kallscheuer, N., Vogt, M., Stenzel, A., Gatgens, J., Bott, M., Marienhagen, J., 2016. Construction of a *Corynebacterium glutamicum* platform strain for the production of stilbenes and (2*S*)-flavanones. Metab. Eng. 38, 47–55.
Kildegaard, K.R., Tramontin, L.R.R., Chekina, K., Li, M., Goedecke, T.J., Kristensen, M., Borodina, I., 2019. CRISPR/Cas9-RNA interference system for combinatorial metabolic engineering of *Saccharomyces cerevisiae*. Yeast 36, 237–247.
Koopman, F., Beekwilder, J., Crimi, B., van Houwelingen, A., Hall, R.D., Bosch, D., van Maris, A.J., Pronk, J.T., Daran, J.M., 2012. *De novo* production of the flavonoid naringenin in engineered *Saccharomyces cerevisiae*. Microb. Cell Factories 11, 155.
Leonard, E., Yan, Y., Fowler, Z.L., Li, Z., Lim, C.G., Lim, K.H., Koffas, M.A., 2008. Strain improvement of recombinant *Escherichia coli* for efficient production of plant flavonoids. Mol. Pharm. 5, 257–265.
Li, H., Gao, S., Zhang, S., Zeng, W., Zhou, J., 2021. Effects of metabolic pathway gene copy numbers on the biosynthesis of (2*S*)-naringenin in *Saccharomyces cerevisiae*. J. Biotechnol. 325, 119–127.
Li, Y., Smolke, C.D., 2016. Engineering biosynthesis of the anticancer alkaloid noscapine in yeast. Nat. Commun. 7, 12137.
Liu, Q., Yu, T., Li, X., Chen, Y., Campbell, K., Nielsen, J., Chen, Y., 2019. Rewiring carbon metabolism in yeast for high level production of aromatic chemicals. Nat. Commun. 10, 4976.
Lv, Y., Marsafari, M., Koffas, M., Zhou, J., Xu, P., 2019. Optimizing oleaginous yeast cell factories for flavonoids and hydroxylated flavonoids biosynthesis. ACS Synth. Biol. 8, 2514–2523.
Lyu, X., Ng, K.R., Lee, J.L., Mark, R., Chen, W.N., 2017. Enhancement of naringenin biosynthesis from tyrosine by metabolic engineering of *Saccharomyces cerevisiae*. J. Agric. Food Chem. 65, 6638–6646.
Manchope, M.F., Casagrande, R., Verri Jr., W.A., 2017. Naringenin: an analgesic and anti-inflammatory citrus flavanone. Oncotarget 8, 3766–3767.
Mans, R., van Rossum, H.M., Wijsman, M., Backx, A., Kuijpers, N.G., van den Broek, M., Daran-Lapujade, P., Pronk, J.T., van Maris, A.J., Daran, J.M., 2015. CRISPR/Cas9: a molecular Swiss army knife for simultaneous introduction of multiple genetic modifications in *Saccharomyces cerevisiae*. FEMS Yeast Res. 15.
Mikkelsen, M.D., Buron, L.D., Salomonsen, B., Olsen, C.E., Hansen, B.G., Mortensen, U. H., Halkier, B.A., 2012. Microbial production of indolylglucosinolate through engineering of a multi-gene pathway in a versatile yeast expression platform. Metab. Eng. 14, 104–111.
Naito, Y., Hino, K., Bono, H., Ui-Tei, K., 2015. CRISPRdirect: software for designing CRISPR/Cas guide RNA with reduced off-target sites. Bioinformatics 31, 1120–1123.
Palmer, C.M., Miller, K.K., Nguyen, A., Alper, H.S., 2020. Engineering 4-coumaroyl-CoA derived polyketide production in *Yarrowia lipolytica* through a beta-oxidation mediated strategy. Metab. Eng. 57, 174–181.
Panche, A.N., Diwan, A.D., Chandra, S.R., 2016. Flavonoids: an overview. J. Nutr. Sci. 5, e47.
Park, S.R., Yoon, J.A., Paik, J.H., Park, J.W., Jung, W.S., Ban, Y.H., Kim, E.J., Yoo, Y.J., Han, A.R., Yoon, Y.J., 2009. Engineering of plant-specific phenylpropanoids biosynthesis in *Streptomyces venezuelae*. J. Biotechnol. 141, 181–188.
Pereira, R., Mohamed, E.T., Radi, M.S., Herrgard, M.J., Feist, A.M., Nielsen, J., Chen, Y., 2020. Elucidating aromatic acid tolerance at low pH in *Saccharomyces cerevisiae* using adaptive laboratory evolution. Proc. Natl. Acad. Sci. U.S.A. 117, 27954–27961.
Rodriguez, A., Chen, Y., Khoomrung, S., Ozdemir, E., Borodina, I., Nielsen, J., 2017. Comparison of the metabolic response to over-production of *p*-coumaric acid in two yeast strains. Metab. Eng. 44, 265–272.
Salehi, B., Fokou, P.V.T., Sharifi-Rad, M., Zucca, P., Pezzani, R., Martins, N., Sharifi-Rad, J., 2019. The therapeutic potential of naringenin: a review of clinical trials. Pharmaceuticals 12.
Shi, S., Chen, Y., Siewers, V., Nielsen, J., 2014. Improving production of malonyl coenzyme A-derived metabolites by abolishing Snf1-dependent regulation of Acc1. mBio 5, e01130, 14.
Srinivasan, P., Smolke, C.D., 2021. Engineering cellular metabolite transport for biosynthesis of computationally predicted tropane alkaloid derivatives in yeast. Proc. Natl. Acad. Sci. U. S. A. 118, e2104460118.
Tartik, M., Liu, J., Mohedano, M.T., Mao, J., Chen, Y., 2023. Optimizing yeast for high-level production of kaempferol and quercetin. Microb. Cell Factories 22, 74.
Tehlivets, O., Scheuringer, K., Kohlwein, S.D., 2007. Fatty acid synthesis and elongation in yeast. Biochim. Biophys. Acta 1771, 255–270.
Tous Mohedano, M., Mao, J., Chen, Y., 2023. Optimization of pinocembrin biosynthesis in *Saccharomyces cerevisiae*. ACS Synth. Biol. 12, 144–152.
Trantas, E., Panopoulos, N., Ververidis, F., 2009. Metabolic engineering of the complete pathway leading to heterologous biosynthesis of various flavonoids and stilbenoids in *Saccharomyces cerevisiae*. Metab. Eng. 11, 355–366.
Wang, G., Moller-Hansen, I., Babaei, M., D'Ambrosio, V., Christensen, H.B., Darbani, B., Jensen, M.K., Borodina, I., 2021. Transportome-wide engineering of *Saccharomyces cerevisiae*. Metab. Eng. 64, 52–63.
Wei, W., Zhang, P., Shang, Y., Zhou, Y., Ye, B.C., 2020. Metabolically engineering of *Yarrowia lipolytica* for the biosynthesis of naringenin from a mixture of glucose and xylose. Bioresour. Technol. 314, 123726.
Wenz, P., Schwank, S., Hoja, U., Schuller, H.J., 2001. A downstream regulatory element located within the coding sequence mediates autoregulated expression of the yeast fatty acid synthase gene *FAS2* by the *FAS1* gene product. Nucleic Acids Res. 29, 4625–4632.
Wu, J., Zhou, L., Duan, X., Peng, H., Liu, S., Zhuang, Q., Pablo, C.M., Fan, X., Ding, S., Dong, M., Zhou, J., 2021. Applied evolution: dual dynamic regulations-based approaches in engineering intracellular malonyl-CoA availability. Metab. Eng. 67, 403–416.
Wu, J., Zhou, T., Du, G., Zhou, J., Chen, J., 2014. Modular optimization of heterologous pathways for *de novo* synthesis of (2*S*)-naringenin in *Escherichia coli*. PLoS One 9, e101492.
Yan, Y., Kohli, A., Koffas, M.A., 2005. Biosynthesis of natural flavanones in *Saccharomyces cerevisiae*. Appl. Environ. Microbiol. 71, 5610–5613.
Zhang, Q., Yu, S., Lyu, Y., Zeng, W., Zhou, J., 2021. Systematically engineered fatty acid catabolite pathway for the production of (2*S*)-Naringenin in *Saccharomyces cerevisiae*. ACS Synth. Biol. 10, 1166–1175.
Zhao, J., 2015. Flavonoid transport mechanisms: how to go, and with whom. Trends Plant Sci. 20, 576–585.
Zhao, J., Dixon, R.A., 2010. The 'ins' and 'outs' of flavonoid transport. Trends Plant Sci. 15, 72–80.
Zhou, S., Lyu, Y., Li, H., Koffas, M.A.G., Zhou, J., 2019. Fine-tuning the (2*S*)-naringenin synthetic pathway using an iterative high-throughput balancing strategy. Biotechnol. Bioeng. 116, 1392–1404.
Zhou, S., Yuan, S.F., Nair, P.H., Alper, H.S., Deng, Y., Zhou, J., 2021. Development of a growth coupled and multi-layered dynamic regulation network balancing malonyl-CoA node to enhance (2*S*)-naringenin biosynthesis in *Escherichia coli*. Metab. Eng. 67, 41–52.
Zhou, Y.J., Gao, W., Rong, Q., Jin, G., Chu, H., Liu, W., Yang, W., Zhu, Z., Li, G., Zhu, G., Huang, L., Zhao, Z.K., 2012. Modular pathway engineering of diterpenoid synthases and the mevalonic acid pathway for miltiradiene production. J. Am. Chem. Soc. 134, 3234–3241.